

Field-induced self assembly: does size matter?

David R. Robinson ^a and Mark Wilson ^a

^a Department of Chemistry, Physical and Theoretical Chemistry Laboratory, University of Oxford, South Parks Road, Oxford OX1 3QZ, U.K.

ARTICLE HISTORY

Compiled April 18, 2018

ABSTRACT

Simulated external electric fields are applied to polarizable species containing either a monodisperse or bidisperse distribution of polarizabilities. The magnitude of the external field and the polarizabilities are systematically varied. The application of an external field (of sufficient magnitude) is found to induce chain formation (as expected). The monodisperse systems are found to “self assemble” with larger induced dipole moments effectively clustering in chains as a result of significant dipole-induced dipole effects. The distribution of the chain lengths are characterised as a function of the applied field and the atom polarizability. For the bidisperse systems the external field induces chain formation and a partial **segregation**, in which the more polarizable species preferentially form chains. The chain lengths are again determined as a function of field strength and the atom polarizabilities. Scaling behaviour is analysed.

1. Introduction.

The study of complex structure formation in dipolar fluids (with or without an applied external field) has a long history (see, for example, the reviews in references [1–7]). The development of both optical- and electron-microscopes has allowed the evolution of these potentially complex structures to be directly observed and characterised [8–24]. The information obtained from these experiments is in stark contrast to the highly spatially- and time-averaged information available from scattering experiments [23–33]. Whilst the ability to observe directly potentially complex assembly behaviour is clearly advantageous, the field of vision is typically limited to a few thousand particles with self-assembly “events” often confined to a relatively small number of independent observations. As a result, mathematical models (which may relate the observed structures to more general property distributions [see, for example, ref. [34]]) and simulation models remain vital interpretative tools. Problems of this sort are particularly attractive theoretically and computationally as the inter-particle interaction energies may often be expressed in relatively simple (and hence computationally-tractable) terms and yet the strongly directional nature of the dipolar interactions may generate a vast richness of structure on a number of (often competing) length-scales [35, 36].

The majority of simulation work to date has assumed the dipoles to be of fixed magnitude and studied their response to the presence of both other dipole moments and/or to an applied field. This class of models is attractive as the interaction energy may

be expressed in a pair-wise additive form, and hence are relatively computationally-tractable, as well as linking more readily to liquid state theories [37, 38]. The simplest systems studied consist of a single species (with fixed dipole magnitude and particle size) [39–52]. An added complexity is to study mixtures of particle types. Examples include the formation of complex structures in simple mixtures of hard-sphere and hard-sphere dipoles [53–58] or mixtures of Lennard-Jones atoms and dipoles [59–65]. Under certain conditions significant **segregation** behaviour is observed (see, for example, refs. [53, 54, 57, 59, 62, 66]). For mixtures of dipole and non-dipolar species the origin of the **segregation** is relatively clear. Above a (temperature-dependent) dipole moment threshold the dipole-dipole interactions are sufficiently strong (compared to interactions involving the non-polar particles) to overcome the entropic mixing contribution to the free energy. Analogous comments apply to mixtures of different magnitudes of dipole [57].

Recent experimental work has focussed on controlling aggregation phenomena on micro- and nano-particle length-scales [8–24]. In these cases dipole moments arise directly from the application of an external field (rather than as a direct consequence of the structure of the particle), that is, moments are *induced* rather than permanent. The applied field may be magnetic or electric meaning that the magnitude of the induced moments is controlled either by the magnetic susceptibility or the dipole polarizability. Aggregation phenomena for systems of this type can be modelled using fixed dipoles with the implicit assumption that the magnitude of the dipole used matches the first order induced moment, that is, any potential many-body dipole-induced dipole (DID) effects are neglected, or incorporated as a mean average. However, the effectiveness of this approach is unclear, in particular in the limit of a high susceptibility and low applied field where such many-body effects may become significant. The role of polarization in systems of this type has been investigated (see, for example, refs. [4, 60, 61, 67, 68] again highlighting potential **segregation** scenarios [69, 70]. **The role of many-body effects in self assembly phenomena has been previously investigated in colloidal systems (see, for example, references [71–73]). In these cases the polarization arises from changes in the colloidal surface charge distribution, the nature of which is dependent upon the colloid size (surface area) and the system dielectric properties. Variation of the relative colloid/solvent dielectric properties along with the colloidal size and charge uncovers a potential richness of formed structures (including chains).**

Furthermore, real particle ensembles would be expected to have a *dispersion* of properties, for example, in terms of both particle diameter and susceptibility. These systems are most commonly (though not exclusively) modelled as monodisperse (for which the appropriate properties represent a mean average) or by directly linking particle diameter and dipole [57, 74]. Significant simulation work has been performed on systems with a polydispersity in dipole strength and/or particle diameter, with the general conclusion that larger particles (higher dipole moments) tend to preferentially aggregate [74–80].

In this paper we study complex structure formation under the influence of an applied electric field. The models employed are fully (dipole) polarizable with dipoles induced both by an external field (whose direction and magnitude may be controlled) and by the presence of other dipole moments (dipole-induced dipole effects) and, as a result, the potential contains a many-body character. Two basic models are employed; in the first monodisperse polarizabilities are employed whilst, in the second, a bidisperse arrangement is selected with the *difference* in polarizabilities varied. Central aims, therefore, are to establish the role (if any) of dipole-induced dipole effects, and the potential implications of the system having a dispersion of polarizabilities.

2. Models and Calculations.

We employ a system comprising polarizable atoms which are physically separated by a purely repulsive short-range potential. No dispersive interactions are included in order to attempt to establish the role of the induced dipole interactions in the formation of any significant structure. The model employed throughout is a pairwise-additive short-range r^{-12} potential,

$$U_{sr}(r) = \frac{4\epsilon\sigma^{12}}{r^{12}}, \quad (1)$$

where $\sigma = 3.405\text{\AA}$ and $\epsilon/k_B = 118\text{K}$. Additional, physically-motivated, terms such as dispersion can be added at a later date.

An external electric field, $\boldsymbol{\epsilon}^{ex}$, is applied (which may vary in both magnitude and direction) and each atom is assigned a (dipole) polarizability, α_i , which is assumed isotropic. As a result the external field may induce a dipole moment on each atom site, $\boldsymbol{\mu}_i = \alpha_i \boldsymbol{\epsilon}^{ex}$.

The total system energy is

$$U = - \sum_i \sum_j \boldsymbol{\mu}_i \mathbf{T}_{ij} \boldsymbol{\mu}_j + \sum_i k_i \mu_i^2 - \sum_i \boldsymbol{\mu}_i \boldsymbol{\epsilon}^{ex} + \sum_i \sum_j U_{sr}(r_{ij}), \quad (2)$$

where

$$\mathbf{T}_{ij} = \frac{1}{r_{ij}^3} \left(\mathbf{I} - \frac{3\mathbf{r}_{ij} \cdot \mathbf{r}_{ij}}{r_{ij}^2} \right), \quad (3)$$

and $k_i = 1/2\alpha_i$. The first term is the dipole-dipole interaction energy, the second term the energy required to polarize atom i , the third term the interaction of the induced dipole with the external field and the final term the total short-range energy. The dipole-dipole term introduces a many-body character into the potential and so the self consistent dipoles must be generated for the starting configuration by solving the dipole-dipole energy iteratively. These dipoles can then be allowed to evolve with the atom dynamics using a Car-Parrinello algorithm which removes the need to further explicit energy minimisation [81–83].

The electric field at each atom site can be expressed as the sum of contributions from the external field and an internal field which arises from the presence of the other dipole moments,

$$\boldsymbol{\epsilon}_i^{int} = \sum_{j \neq i} \mathbf{T}_{ij} \boldsymbol{\mu}_j. \quad (4)$$

As a result,

$$\begin{aligned} \boldsymbol{\mu}_i &= \alpha_i (\boldsymbol{\epsilon}^{ex} + \boldsymbol{\epsilon}_i^{int}), \\ &= \boldsymbol{\mu}^{ex} + \alpha_i \boldsymbol{\epsilon}_i^{int} = \boldsymbol{\mu}^{ex} + \boldsymbol{\mu}_i^{int}. \end{aligned} \quad (5)$$

As a result, by varying the relative magnitudes of $|\boldsymbol{\epsilon}^{ex}|$ and $\{\alpha_i\}$ the relative contributions of the two terms in equation 5 can be varied. For example, if we work at constant

$|\mu_i^{ex}|$ ($\equiv \alpha_i \epsilon^{ex}$) then high fields require small polarizabilities to generate $|\mu_i^{ex}|$ which mean that the dipole-induced dipole (DID) term (the second term in equation 5) will be small compared with μ^{ex} . Conversely, small fields require high polarizabilities and so the DID term may become significant compared with μ^{ex} . Two models are considered here. In the first a monodisperse polarizability distribution is used (*i.e.* $\alpha_i = \alpha$). In the second a bidisperse distribution of polarizabilities is applied in which half of the atoms are assigned one polarizability, α_1 and the remaining half another, α_2 , the difference (polarizability contrast) given by $\Delta\alpha = \alpha_2 - \alpha_1$.

Starting configurations are generated by performing molecular dynamics simulations on the fluid phase at zero external field. Configurations are then extracted from the equilibrium fluids at time separations significantly greater than the characteristic system relaxation time (as determined from the intermediate scattering functions). The result is that successive configurations can be considered as effectively independent. Each configuration is then quenched to $T \sim 50K$ by the application of Nosé-Hoover thermostats [84, 85]. **The temperature chosen is low enough so as to be below any realistic glass transition temperature.**

Calculations are performed at varying fields ($0 < |\epsilon| < 0.25au$) and polarizabilities, keeping $\alpha\epsilon^{ex}$ fixed at $0.5au$. In all cases the mean dipole, in the absence of DID effects, $\bar{\mu} = \bar{\alpha}\epsilon^{ex}$, is held constant (where $\bar{\alpha}$ is the mean polarizability). As a result, a number of different trends and potential scaling relationships can be investigated, for example, following fixed $\Delta\alpha$, $\bar{\alpha}$, or $\frac{\Delta\alpha}{\bar{\alpha}}$.

3. Results.

The results are divided into those for the monodisperse (all atoms with equal polarizability) and bidisperse (two sets of polarizabilities) systems.

3.1. Monodisperse Polarizability.

3.1.1. Dipole Distributions.

Figure 1 shows the distribution of dipole moment magnitudes obtained from the final quenched configurations. As the field strength is reduced (and hence the dipole polarizabilities increased to maintain a fixed μ^{ex}) the DID terms become more significant and the mean dipole moment increases (as shown in the inset to figure 1). The inset to figure 1 shows the mean dipole moment, $\bar{\mu}$, as a function of the applied field. For a two-atom cluster with atoms separated by a distance r the first-order dipole-induced dipole is given by

$$\mu_{(1)}^{DID} = \frac{2\alpha\mu^{ex}}{r^3} \equiv \frac{2\alpha^2\epsilon^{ex}}{r^3}, \quad (6)$$

where α is the atom polarizability. Since both atoms in the pair are polarizable then iterative equations must be solved in order to determine the self-consistent dipole, $\mu_{(\infty)}^{DID}$. For a chain of dipoles the field on a given atom due to the dipoles resident on

the atoms in the chain is given by

$$\begin{aligned}
\epsilon &= \frac{4\alpha\epsilon^{ex}}{r^3} + \frac{4\alpha\epsilon^{ex}}{(2r)^3} + \dots \\
&= \frac{4\alpha\epsilon^{ex}}{r^3} \left\{ 1 + \frac{1}{8} + \frac{1}{27} + \dots \right\}, \\
&= \frac{4\alpha\epsilon^{ex}}{r^3} \sum_{n=1}^{\infty} n^{-3}, \\
&= \frac{4\alpha\epsilon^{ex}}{r^3} \zeta(3),
\end{aligned} \tag{7}$$

where the “4” arises from the chains of dipoles percolating in two directions from a given site and $\zeta(3)$ is a Riemann zeta function (also known as Apéry’s constant) having a value of $\zeta(3) \simeq 1.2021$. As a result, the first-order DID dipole term for a chain is given by

$$\mu_{(1)}^{DID} = \frac{4\alpha^2\epsilon^{ex}\zeta(3)}{r^3}, \tag{8}$$

and $\mu_{(\infty)}^{DID}$ can be generated by subsequent iterations. Since μ^{ex} is fixed ($= \alpha\epsilon^{ex}$) we can write the above equation as

$$\mu_{(1)}^{DID} = \frac{4\mu_{ex}^2\zeta(3)}{r^3} \frac{1}{\epsilon^{ex}}, \tag{9}$$

which shows that the DID term should scale inversely to the applied field if significant chain structures are formed.

The inset to figure 1 shows both the first-order corrected and self consistent dipoles predicted for a pair of atoms and for an infinite chain. The separation r is taken as the first peak position in the pair distribution function. At low ϵ^{ex} (high α) the observed mean dipole “shifts” from sitting on the two-atom curve to sitting on the infinite chain curve, indicative of the formation of significant chains at low ϵ^{ex} .

There is a limit on the magnitude of the polarizability which can be applied. Once $\mu_{(1)}^{DID} \geq \mu_{ex}$ then the DID terms are too large for convergence to a self consistent value (a “polarization catastrophe”). The “critical” polarizability, α^* , can be evaluated as

$$\begin{aligned}
\alpha^*\epsilon &= \alpha^*\epsilon^{ex} \\
\frac{4\alpha^*\epsilon^{ex}}{r^3}\zeta(3) &= \epsilon^{ex},
\end{aligned} \tag{10}$$

and so,

$$\alpha^* = \frac{r^3}{4\zeta(3)}. \tag{11}$$

Notice that the critical polarizability is independent of ϵ^{ex} but depends on the nearest-neighbour particle separation, For a separation of the order of $r \sim 6\text{au}$, for example, $\alpha^* \simeq 45\text{au}$.

3.1.2. Structure.

Figure 2 shows a molecular graphics “snapshot” for two fields, $\epsilon^{ex} = 0.025\text{au}$ and $\epsilon^{ex} = 0.25\text{au}$, again at constant μ^{ex} . In both cases clear chain-like structures form in which the major component of each dipole lines up with the applied field. The chain structures arise from the presence of the dominant (attractive and highly anisotropic) dipole-dipole interactions and appears more ordered in the low field case, reflecting the larger dipoles present as a result of the larger DID interactions (figure 1). To quantify the degree of ordering figure 3 (upper panel) shows the half width half maximum for the bond angle distributions obtained for the X-X-X triplets comprising the chains as a function of the applied field. At low field (high polarizability) the width of the peak centred at $\theta = 180^\circ$ (corresponding to the presence of linear chains) is significantly less than that at high field (low polarizability).

The above analysis highlights the mean chain length as an important metric. The mean chain length, \bar{c} , may be generated in a number of ways which, in ideal cases, will be equivalent, but which may differ in, for example, their treatment of the effect of boundary conditions or the presence of “defect” (here meaning “non-chain-like”) coordination environments. One method is to relate \bar{c} to the mean coordination number, \bar{n} ,

$$\bar{n} = \frac{\sum_i i n_i}{\sum_i n_i}, \quad (12)$$

where n_i is the number of atoms of coordination number i . If we assume all atoms to be 0-, 1- or 2-coordinate (*i.e.* forming chains only) then,

$$\bar{n} = \frac{2n_2 + n_1}{n_2 + n_1 + n_0}. \quad (13)$$

In this model each chain is made from 2-coordinate atoms “book-ended” by single-coordinate atoms. As a result,

$$\bar{c} = \frac{\left(\frac{n_1}{2}\right) \left(\frac{n_1+n_2}{n_1/2}\right) + n_0}{(n_1/2) + n_0} = \frac{n_0 + n_1 + n_2}{(n_1/2) + n_0}, \quad (14)$$

where the first term represents the average of the $(n_1/2)$ chains formed and the 0-coordinate single-atom “chains”. Combining equations 13 and 14 to eliminate n_2 gives

$$\bar{c} = 1 + \frac{N\bar{n}}{2n_0 + n_1}, \quad (15)$$

where $N = n_0 + n_1 + n_2$. The fraction of n -coordinate sites is $f_n = n_n/N$ and so

$$\bar{c} = 1 + \frac{\bar{n}}{2f_0 + f_1}. \quad (16)$$

Alternatively, one may determine the chain lengths directly. In some ways defining a chain length is analogous to the problems in defining rings (see the definition of Gutmann, King’s and primitive rings discussed in, for example [86]). One option (essentially a “shortest chain approximation”) is to count all non-two-coordinate units as chain termini. For chains constructed from only 0, 1 and 2-coordinated particles

the definition is clear with two-coordinate atoms forming the chain “body” and singly-coordinate atoms the termini. There are potential problems if the chains become effectively infinite (because of the boundary conditions) but these effects can be estimated by determining the distributions with and without the boundary conditions (see below). If there are sites with coordination number $n > 2$ then the algorithm treats higher coordinate sites as termini. For example, the small cluster shown in figure 4 will be broken down into two chains with four particles and one with six. Alternative definitions are, of course, possible. The advantage of the algorithm outlined here is that only the atoms with a coordination number greater than two appear in more than one chain, and even then only as the chain terminus.

Figure 3 (lower panel) shows the mean chain lengths, determined as a function of the applied field, determined from both the mean coordination number (equation 16) and directly from the chain length distributions. At high field (low α) the mean chain lengths are relatively small and those generated from the two methods are in good agreement. Significantly, we will show elsewhere that the growth of the chains can be understood in terms of a compound Poisson process *if* the 0-coordinate sites are included in the summations [34, 87]. As the field is increased (α reduced) the mean chain length rises substantially (as can be seen by eye for the single configurations shown in figure 2). At the lowest fields the mean chain lengths calculated directly and from the mean coordination number start to diverge. The divergence is simply a reflection of the formation of effectively infinite chains (which percolate across the whole simulation cell). The mean chain size, defined in terms of \bar{n} in equation 16, will diverge to infinity if all chains percolate across the simulation cell (as both f_0 and f_1 will become zero). The “dip” at $\epsilon = 0.02\text{au}$ on \bar{c} generated from the direct chain counting arises from chains which have become effectively infinite (percolating across the cell) from being lost from the count (as there are no termini atoms to identify). The effect of this loss can be estimated by calculating \bar{c} in the absence of the periodic boundary conditions (*i.e.* effectively forcing atoms at the cell edges to become termini). Figure 3(b) shows the effects of applying this approximation. Removing the boundary conditions reduces \bar{c} except at the lowest ϵ (where the largest number of chains percolate across the cell). However, as shown elsewhere [34] the growth statistics which underpin the chain growth itself may onto a relatively simple distribution (which agrees with that observed directly from experimental studies) and, as a result, system size effects are insignificant in the sense that these distributions may be used to determine \bar{c} *without* recourse to further simulation.

3.1.3. Coordination Environments.

In order to identify any further ordering within the chains themselves we “colour” atoms in terms of the magnitudes of their dipole moments. The upper 25% of a distribution in figure 1 are coloured “A” and the remaining 75% coloured “B”. The local coordination environments are then characterised by comparing the observed coordination numbers (A-A, A-B, B-A and B-B) to those expected from a random distribution, $\Delta p_A(k) = p_A^{sim}(k) - p_A^{rnd}(k)$, where

$$p_A^{rnd}(k) = \frac{n!}{k!(n-k)!} p^k (1-p)^{n-k}, \quad (17)$$

and $p_A^{sim}(k)$ is the fraction of atoms A with coordination k obtained directly from the simulations. For the chain structures $n = 2$ and so, for atoms coloured A at the centre,

the options are AAA, AAB, BAA and BAB (random probabilities 1/16, 3/16, 3/16 and 9/16 respectively).

Figure 5(a) shows $\Delta p_A(k)$ determined as a function of the external field. A larger dipole is significantly more likely to be found adjacent to another large dipole ($\Delta p_A(2)$ is positive, corresponding to the presence of AAA units, $\Delta p_A(0)$ is negative, corresponding to a relative dearth of BAB units). Furthermore this preference becomes more prominent at low field (high polarizability). The locations of the two sets of coloured atoms are shown in figure 2 for two snapshots corresponding to the high and low field “limits”. The presence of significant AAA chains is clear in both cases though more obvious at low field. Figure 5(b) shows the total mean chain lengths along with those calculated from the AA and BB pairs only (as determined from equation 16). At high field (low α) the chains which form are relatively short ($\bar{c} \sim 3$) and are dominated by particles housing the larger dipole moments. Note that the mean AA.. chain length, \bar{c}_{AA} is larger than the total mean chain length as the latter contains contributions from the B subsystem which contains significant numbers of small chains. At low field (high α) *both* the AA and BB chains increase in mean length although the AA chains still dominate.

In summary, therefore, the system appears to “self assemble” in terms of the distribution of the low and high dipole moments. The effect is more pronounced at high α as the mean dipole moments increase (as seen in figure 1) as a direct result of the strength of the DID term (which acts to weight μ_i strongly in comparison to the term from μ_{ex} in equation 5).

3.2. Bidisperse Polarizability Distribution.

The above analysis for systems with monodisperse polarizability distributions suggests an effective **segregation** in terms of the magnitudes of the induced dipole moments. To further probe any potential **segregation** we study a range of systems in which equal numbers of atoms have different polarizabilities, $\{\alpha_1, \alpha_2\}$, characterised by the mean polarizability, $\bar{\alpha} = (\alpha_1 + \alpha_2)/2$ and polarizability contrast, $\Delta\alpha = \alpha_1 - \alpha_2$.

3.2.1. Dipole Distributions.

Figure 6 shows the distribution of dipole moment magnitudes for the bidisperse systems at fixed applied external field, $\epsilon^{ex} = 0.05\text{au}$, with different pairs of atom polarizabilities $\{\alpha_1, \alpha_2\}$ chosen such that $\bar{\alpha}\epsilon^{ex}$ is fixed at 0.5au . The majority of the observed dipoles show a DID enhancement as evidenced by the mean dipoles, with the more polarizable species showing the greatest enhancement. To highlight this the inset to the figure shows the “excess” (DID) dipole ($\equiv \bar{\mu} - \alpha_X \epsilon^{ex}$, $X = \{1, 2\}$) as a function of polarizability. The most polarizable species considered here ($\alpha_1 = 13$ or 15au) show a clear “three peak” structure in the dipole distribution. For example, for $\alpha_1 = 15\text{au}$ the distribution shows peaks at $\bar{\mu} = 0.77, 0.90$ and 1.05au respectively

3.2.2. Structure.

Figure 7 shows molecular graphics “snapshots” of three of the bidisperse configurations for the fixed external field of $\epsilon^{ex} = 0.05\text{au}$ and for $\{\alpha_1, \alpha_2\} = \{15, 5\}\text{au}$, $\{13, 7\}\text{au}$ and $\{11, 9\}\text{au}$ respectively. All three configurations show clear chain structure. To further break down the origin of these structures the atoms are again coloured, this time simply in terms of their respective polarizabilities (with the higher polarizability

atoms labelled “A” and the lower “B”). As a result, it is clear from the figure that, for $\{\alpha_1, \alpha_2\} = \{15, 5\}$ au the more polarizable atoms form well-defined chains with the less polarizable atoms forming less well-defined structures. For the $\{\alpha_1, \alpha_2\} = \{11, 9\}$ au configuration the chain structure is more evident in both sublattices although the chains appear less aligned with ϵ^{ex} compared to the more polarizable atoms in the $\{\alpha_1, \alpha_2\} = \{15, 5\}$ au configuration.

The inset to figure 6 shows the dipoles predicted for a given polarizability for an infinite chain and a two-atom pair (both calculated as the first order correction, $\mu_{(1)}^{DID}$, and the self-consistent correction, $\mu_{(\infty)}^{DID}$). The calculated mean dipole moments show a clear “upturn” at high α indicative of significant chain formation with the chain composition dominated by the high α species. For example, for a chain consisting of a single species only, the first order DID would be given by equation 8 (or equation 9) with α as the polarizability of the single species making up the chain. The inset to figure 6 highlights that, at the highest polarizabilities studied, the observed dipoles agree with those predicted from equation 8, demonstrating that the chains formed are, firstly, relatively long and, secondly, dominated by a single (high polarizability) species. As the polarizability is reduced the dipoles become smaller than these limiting values indicating that the chains formed contain a greater number of the lower polarizability species.

Having established that the high polarizability contrast systems appear dominated by chains constructed from the higher polarizability atoms, the origin of the three peak structure in the dipole moment distribution (figure 6) can now be fully rationalised. For first order chains comprised of the more polarizable species only, the dipole-induced dipoles for the 0-, 1- and 2-coordinate atoms would be zero, $2\alpha^2\epsilon^{ex}\zeta(3)/r^3$ and $4\alpha^2\epsilon^{ex}\zeta(3)/r^3$ respectively (see equation 8), where we assume both the 1- and 2-coordinate sites form part of long chains. The peak positions in $n(\mu)$ for, for example, $\alpha_1 = 15$ au correspond to these predicted values. For chains composed of a mixture of the two atom types effective mean field values (which would be smaller) would be predicted.

To clarify what is meant by a “long” chain consider the following. The (first-order) electric field on a singly coordinate atom (labelled “1”) on the end of an infinite chain will be given by

$$\epsilon_1 = \frac{2\alpha\epsilon^{ex}}{r^3}\zeta(3), \quad (18)$$

whilst the field on the neighbouring (two-coordinate) atom will be

$$\epsilon_2 = \epsilon_1 + \frac{2\alpha\epsilon^{ex}}{r^3}. \quad (19)$$

As a result, for the n^{th} atom in the chain,

$$\epsilon_n = \epsilon_{n-1} + \frac{2\alpha\epsilon^{ex}}{[(n-1)r]^3}. \quad (20)$$

The dipoles reach their saturated infinite chain value relatively rapidly as the chain length increases, for example, reaching $> 95\%$ of the limiting value when $n = 3$. As a result, the dipole distributions differentiate very clearly between the zero, one and two-coordinate sites.

Figure 8 shows the respective HWHM for the bond angle distributions calculated for all atoms as a function of both (a) ϵ_{ex} and (b) $\Delta\alpha$. As the field is reduced the peaks become significantly broader indicative of the formation of relatively disordered chains whose bond vectors are less aligned with the external field vector compared to high field. At high field the peaks become narrow as the induced dipole-dipole interactions dominate and the chains effectively line up with the external field vector. As the polarizability contrast increases (higher $\Delta\alpha$) the peaks become narrower. These results hint that the chains formed are dominated by the higher polarizability species.

3.2.3. Scaling with the external field.

Figure 7 demonstrates that significant chain formation occurs over a range of parameter space. We need to establish how the structure of these chains (composition, length...) varies as a function of both the applied field and the internal system parameters (polarizabilities). Furthermore, one might expect the structural properties to scale, perhaps in terms of the product of the polarizability and the field.

To quantify any significant structural differences we again calculate $\Delta p_A(k)$ with the atom type A and B defined purely in terms of their polarizability (rather than the magnitude of the dipole moment in the context of the distribution of moments). This does retain the possibility that, when considering two atoms of different polarizability, the atom with the higher polarizability may house the lower moment, depending upon the detail of the surrounding environment. The probability of this occurring will clearly decrease with increasing polarizability contrast. Figure 9(a) shows $\Delta p_A(k)$ [$k = 0, 1, 2$] as a function of the applied field for a range of $\{\alpha_1, \alpha_2\}$ for $\bar{\alpha} = 10\text{au}$. At low fields $\Delta p_A(k) \sim 0$ reflecting a lack of chain formation. As the field increases $\Delta p_A(2)$ becomes positive (and $\Delta p_A(0)$ becomes negative) indicating a preferred formation of ...AAA... chains, that is, chains comprising the more polarizable species. The $\Delta p_A(0)$ and $\Delta p_A(1)$ functions effectively mirror $\Delta p_A(2)$ since the preferential formation of AAA chains ($\Delta p_A(2)$ positive) must be associated with the relative lack of the AAB or BAB units. These functions show some interesting behaviour as a function of the *difference* between the two constituent polarizabilities, $\Delta\alpha = \alpha_2 - \alpha_1$. For large $\Delta\alpha$, $\Delta p_A(2)$ increases and reaches a plateau at the high field limit indicating the AAA-dominated chains to be stable to high field. For small $\Delta\alpha$ all of the $\Delta p_A(k)$ functions tend to zero **in the high field limit** (as expected for the limit that $\Delta\alpha \rightarrow 0$ as the two species become equivalent). Potentially the most interesting behaviour is displayed at intermediate values of $\Delta\alpha$. In these cases $\Delta p_A(2)$ shows a maximum at $\epsilon^{ex} \sim 0.05\text{au}$ ($\equiv \bar{\mu} = \bar{\alpha}\epsilon^{ex}$) indicating that there is a range of applied fields for which there is *greater* preference for AAA-chain formation compared with that at the high field limit.

Figure 9(b) shows the analogous functions for $\bar{\alpha} = 5\text{au}$. In these cases the applied field required to induce preferential AAA-chain formation is greater than for $\bar{\alpha} = 10\text{au}$, although the functions appear to display the same basic structure with, for example, maxima in $\Delta p_A(2)$. The analogous $\Delta p_B(2)$ functions (not shown) compliment those for $\Delta p_A(2)$. At intermediate field strengths the number of BBB units is at a maximum ($\Delta p_B(2) > 0$) reflecting the fact that the A particles are effectively unavailable for chain formation, being already part of A-dominated chain units.

The $\Delta p_A(k)$ functions shown in figure 9, determined at different $\bar{\alpha}$, might be expected to scale onto each other **purely** in terms of $\bar{\alpha}$ (**recalling that both** $\bar{\mu} = \bar{\alpha}\epsilon^{ex}$ in the absence of DID effects). Figure 9(c) shows the $\Delta p_A(2)$ functions only (as $\Delta p_A(0)$ and $\Delta p_A(1)$ mirror these - figures 9(a) and (b)) with the abscissa axis scaled for $\bar{\alpha}$.

The data sets for $\bar{\alpha} = 5\text{au}$ and $\bar{\alpha} = 10\text{au}$ scale onto each other reasonably well. There is, however, a systematic shift to lower $\epsilon\bar{\alpha}$ as $\bar{\alpha}$ increases which may be rationalised as a DID effect. To demonstrate **this effect** figure 9(d) shows the same functions scaled by an “effective” polarizability, $\alpha_{(1)}^{eff}$, **defined as** the polarizability required to reproduce the total dipole moments including the first order DID correction,

$$\begin{aligned}\mu_{(1)} &= \mu^{ex} + \mu_{(1)}^{DID} \\ &= \mu^{ex} + \frac{4\alpha^2\epsilon^{ex}\zeta(3)}{r^3} = \alpha_{(1)}^{eff}\epsilon^{ex},\end{aligned}\quad (21)$$

where r is the nearest-neighbour particle separation. As a result,

$$\frac{\alpha_{(1)}^{eff}}{\alpha} = \left(1 + \frac{4\alpha\zeta(3)}{r^3}\right), \quad (22)$$

and so the ratio of the effective polarizability **and** the actual polarizability scales linearly with increasing α for the first order DID correction. Figure 9(d) shows the $\bar{\alpha} = 5\text{au}$ and $\bar{\alpha} = 10\text{au}$ data scaled by $\alpha_{(1)}^{eff}$. The increase in $\Delta p_A(2)$ at low field and the location of the peak **in the same function** now map onto each other very well.

To further understand how the chain structures vary with system figure 10(a) shows the mean chain lengths, \bar{c} , constructed from the high polarizability species (A) only as a function of $\{\alpha_1, \alpha_2\}$ and ϵ^{ex} **and for which $\bar{\alpha} = 10\text{au}$** . For contrast the equivalent **chain lengths obtained for the** monodisperse system is also shown. **For the monodisperse system** the high field mean chain length reaches a simple statistical limit of $\bar{c} = 2$ (equation 16). As would be expected \bar{c}_{AA} mirrors $\Delta p_A(2)$, showing a clear peak at $\epsilon = 0.05\text{au}$. Figure 10(b) shows the mean chain lengths constructed from the high polarizability species (A) for $\bar{\alpha} = 5\text{au}$. The trends in chain length match those for $\bar{\alpha} = 10\text{au}$ **(figure 10(a))** with a maximum at $\epsilon^{ex} \sim 0.1\text{au}$, again matching that in $\Delta p_A(2)$ in figure 9(b).

Figures 10(c) and (d) show the mean chain lengths constructed from the high polarizability species (A) scaled with $\bar{\alpha}$ and α_{eff} for $\bar{\alpha} = 5$ and 10au respectively. The peak positions **appear to** scale better with α_{eff} than with $\bar{\alpha}$ although the peak heights do not, with the more polarizable species showing longer chains formed. We will consider this difference **further** below.

3.2.4. Scaling with the polarizability contrast, $\Delta\alpha$.

Figure 11(a) shows $\Delta p_A(k)$ calculated as a function of the polarizability contrast between the two species, $\Delta\alpha = \alpha_1 - \alpha_2$, at different combinations of **the mean polarizability and the external field**, $\bar{\alpha}$ and ϵ^{ex} (such that $\bar{\alpha}\epsilon^{ex}$ is again held fixed). In all cases the fraction of AAA chains increases as $\Delta\alpha$ increases **demonstrated** by the increase in $\Delta p_A(2)$ with concomitant decreases in both $\Delta p_A(1)$ and $\Delta p_A(0)$ indicating that the degree of **segregation** of the A and B sublattices is dependent upon the contrast in induced dipole moments.

Figure 11(b) shows the corresponding functions centred on the “B” atoms (those of lower polarizability). In a broad sense these functions mirror those centred on particle A (figure 11(a)) with an excess in $\Delta p_B(0)$ correlated with negative values for both $\Delta p_B(2)$ and $\Delta p_B(1)$, corresponding to a relative lack of B-B nearest neighbours in the chains. Weak turning points are displayed in $\Delta p_B(2)$ and $\Delta p_B(0)$ indicating that,

at the highest polarizability contrast, the dipoles induced on the A atoms are large enough so as to preclude B atoms sitting in the chains. Analogous many-body effects are observed in related colloidal systems [71].

3.2.5. Scaling with $\Delta\alpha/\bar{\alpha}$.

Further to our consideration of how the system properties vary with applied field and polarizability contrast, we now consider how these properties vary with the ratio of the polarizability contrast and the mean polarizability. Such a scaling can be considered in terms of a two-state model. In a two state model [88–90] an equilibrium is established between two species A and B with the free energy of mixing given by

$$\Delta G = RT[x_A \ln(x_A) + (1 - x_A) \ln(1 - x_A)] + W x_A (1 - x_A), \quad (23)$$

where x_A is the mole fraction of species A and W is a non-ideal mixing parameter. W can be expressed in terms of the difference in the interaction energies of the like-like and like-unlike terms. In this case the dominant interactions are the those acting between induced dipoles and so we can write,

$$W = \beta(\mu_1^2 + \mu_2^2 - 2\mu_1\mu_2)r^{-3}. \quad (24)$$

Now, $\mu_i = \alpha_i \epsilon$ and so

$$\begin{aligned} W &= \beta \epsilon^2 (\alpha_1^2 + \alpha_2^2 - 2\alpha_1\alpha_2) r^{-3} \\ &= \beta \epsilon^2 (\alpha_1 - \alpha_2)^2 r^{-3} = \beta \epsilon^2 \Delta\alpha^2 r^{-3}. \end{aligned} \quad (25)$$

Now, $\bar{\mu} = \bar{\alpha} \epsilon$ and so

$$W = \beta \bar{\mu}^2 \left\{ \frac{\Delta\alpha}{\bar{\alpha}} \right\}^2 r^{-3}, \quad (26)$$

which indicates a scaling in terms of $\Delta\alpha/\bar{\alpha}$ to be appropriate.

Figures 12(a) and (b) show $\Delta p_A(k)$ and $\Delta p_B(k)$ with the x -axis scaled by $\{\frac{\Delta\alpha}{\bar{\alpha}}\}$. As anticipated from a two-state model the curves generated at different combinations of $\bar{\alpha}$ and ϵ^{ex} fall onto an approximate universal curve. To emphasize this point figure 13 shows the scaling procedure for $\Delta p_A(2)$ only. Figures 13(a) and (b) show the scaling in terms of $\bar{\alpha}$ whilst figures 13(c) and (d) show the scaling in terms of the effective polarizability, $\alpha_{(1)}^{eff}$ as discussed above. **The scaling in terms of the effective polarizability is the most impressive.**

3.2.6. Ramping and Quenching

. To further understand the factors controlling the atomistic detail of the chain formation, additional simulations are performed in which the external field is systematically increased and decreased (“ramped” up and down) starting from the isotropic (zero field) configurations. Molecular dynamics are performed for 10000 steps at a given field strength after which the field is increased (or decreased) by $\Delta\epsilon = 0.005\text{au}$. Figure 14 shows $\Delta p_A(2)$ (the “excess” AAA units in the chains) as a function of the external field for $\{\alpha_1, \alpha_2\} = \{13, 7\}$ and $\{12, 8\}\text{au}$ respectively. In both cases two “regimes” can be identified. At intermediate strength fields (around the magnitude of field required

to show a maximum in $\Delta p_A(2)$ for the quenched configurations, ϵ^*) the quenched configurations show chains with a greater number of A particles (higher α) compared with those generated via field ramping. At high fields the effect is reversed with the ramped configurations showing the greater number of A particles. An inspection of the energetics, both for the quench- and ramp-generated configurations, reveals only subtle differences. For $\{\alpha_1, \alpha_2\} = \{12, 8\}$ au at $\epsilon \sim \epsilon^*$ the quenched configurations are more stable by $\Delta U \sim 0.18 \text{kJmol}^{-1}$, rising to $\sim 0.40 \text{kJmol}^{-1}$ for $\{\alpha_1, \alpha_2\} = \{13, 7\}$ au. At high fields ($\epsilon > \epsilon^*$) the energetic balance is reversed with energy differences of $\Delta U \sim 0.47 \text{kJmol}^{-1}$ and $\sim 1.50 \text{kJmol}^{-1}$ respectively. These energy differences are relatively small for these systems. For example, the dipole-dipole energy for an isolated atom pair with $\alpha = 10$ au and $\epsilon = 0.05$ au is of the order of 6kJmol^{-1} and of the order of 15kJmol^{-1} for an infinite chain. The result is that the energy landscape associated with the chain formation is relatively “rugged” with numerous local energy minima (corresponding to different chain conformations and chain length distributions) within a very narrow energy range. As a result, the broad method by which the chains are formed (here by quenching at fixed field or by a systematic change in the applied field) is significant. Furthermore, there is no reason to believe that these differences would not translate into the experimental regime. In the present case the application of a large field to isotropic configurations results in more disordered chains than those generated by ramping up the field. The large dipoles generated allow the particles to effectively “grab” a nearest-neighbour atom and, given the relatively strong dipole-dipole interactions, the particles are generally able to hold onto these species regardless of their physical identity. At $\epsilon \sim \epsilon^*$ the energies of interaction are such that the more polarizable species are able to swap with less polarizable species which become “trapped” in the forming chains.

The energetic stability of the chains formed from ramping the external field is highlighted when the field is systematically ramped back down to zero. The relatively long chains are retained until $\epsilon \simeq \epsilon^*$, that is, there is a significant hysteresis in the chain formation centred around $\epsilon \sim \epsilon^*$.

4. Discussion and Conclusions.

In this paper dynamic chain formation, resulting from an applied external electric field, has been studied for systems of polarizable species with no permanent moments. The external field induces dipoles on each particle which interact highly anisotropically to favour chain-formation in a relatively well-understood manner for particles with permanent dipole moments. The study of induced, rather than permanent, dipole moments adds a further degree of freedom in that the dipoles may be induced both by the applied (external) electric field and by the internal field resulting from the presence of other dipoles in the system (dipole-induced dipoles). The relative magnitudes of the internal and external fields can be controlled. For systems with a monodisperse polarizability distribution dipole-induced dipole effects are significant in promoting the formation of well-ordered chains aligned with the external field, in particular in systems containing highly polarizable species. For systems with a bidisperse polarizability distribution the application of an external field leads not only to chain formation, but also to significant **segregation**. Furthermore, there appears to be a critical range of field magnitudes over which the degree of **segregation** is maximised.

5. Acknowledgements.

It is a pleasure to acknowledge the enormous contribution of Professor Frenkel to international science. The authors thank the EPSRC (EP/J001902/1) for financial support.

References

- [1] C.Holm and J.-J.Weis, Curr. Opin. Coll. Int. Sci. **10**, 133 (2005).
- [2] S.H.L.Klapp, J.Phys.: Condens. Mat. **17**, R525 (2005).
- [3] B.Huke and M.Luecke, Rep. Prog. Phys. **67**, 1731 (2004).
- [4] B.J.Alder and E.L.Pollock, Ann. Rev. Phys. Chem. **32**, 311 (1981).
- [5] A.F.Bakuzis, L.C.Branquinho, L. e Castro, M. de Amaral e Eloí and R.Miotto, Adv. Coll. Int. Sci. **191-192**, 1 (2013).
- [6] J. de Vincente, D.J.Klingenberg and R.Hidalgo-Alvarez, Soft Matter **7**, 3701 (2011).
- [7] H. Loewen, J. Phys.: Condens. Mat. **20**, 404201 (2008).
- [8] G.Helgesen, A.T.Skjeltorp, P.M.Mors, R.Botet and R.Jullien, Phys. Rev. Lett. **61**, 1736 (1988).
- [9] M.Fermigier and A.P.Gast, J. Coll. Int. Sci. **154**, 522 (1992).
- [10] J.H.E.Promislow, A.P.Gast and M.Fermigier, J. Chem. Phys. **102**, 5492 (1995).
- [11] A.T.Skjeltorp, J. Appl. Phys. **57**, 3285 (1985).
- [12] P.Dominguez-Garcia, S.Melle, J.M.Pastor and M.A.Rubio, Phys. Rev. E **76**, 051403 (2007).
- [13] P.Dominguez-Garcia, J.M.Pastor and M.A.Rubio, Eur. Phys. J. E **34**, 36 (2011).
- [14] J.Cernak and G.Helgesen, Phys.Rev.E **78**, 061401 (2008).
- [15] J.Cernak, G.Helgesen and T.Skjeltorp, Phys.Rev.E **70**, 031504 (2004).
- [16] R.M.Erb, M.D.Krebs, E.Alsberg, B.Samanta, V.M.Rotello and B.B.Yellen, Phys.Rev.E **80**, 051402 (2009).
- [17] G.Pal, F.Kun, I.Varge, D.Sohler and G.Sun, Phys.Rev.E **83**, 061504 (2011).
- [18] F.Martinez-Pedrero, A.El-Harrak, J.C.Fernandez-Toledano, M-Tirado-Miranda, A.Schmitt, J.Bibette and J.Callejas-Fernandez, Phys.Rev.E **78**, 011403 (2008).
- [19] F.Martinez-Pedrero, M-Tirado-Miranda, A.Schmitt and J.Callejas-Fernandez, Phys.Rev.E **76**, 011405 (2007).
- [20] R.E.Moctezuma, F.Donado and J.L.Arauz-Lara, Phys.Rev.E **88**, 032305 (2013).
- [21] T.Ukai, H.Morimoto and T.Maekawa, Phys.Rev.E **83**, 061406 (2011).
- [22] S.Melle, O.G.Calderon, M.A.Rubio and G.G.Fuller, Phys.Rev.E **68**, 041503 (2003).
- [23] D.Sohn, J. Mag. Mag. Mat. **173**, 305 (1997).
- [24] F.Martinez-Pedrero, M-Tirado-Miranda, A.Schmitt and J.Callejas-Fernandez, J. Chem. Phys. **125**, 084706 (2006).
- [25] R.Rosman, J.J.M.Janssen and M. Rekveldt, J. Mag. Mag. Mat. **85**, 97 (1990).
- [26] G.Meriguet, E.Dubois, M.Jardat, A.Bourdon, G. Demouchy, V.Dupuis, B.Farago, R.Perzynski and P.Turq, J. Phys.: Condens. Mat. **18**, S2685 (2006).
- [27] P.C.Jordan, Mol. Phys. **25**, 961 (1973).
- [28] S.Melle, M.A.Rubio and G.G.Fuller, Phys.Rev.Lett. **87**, 115501 (2001).
- [29] J.E.Martin and J.Odinek, J. Non-Cryst. Solids. **172-174**, 1135 (1994).
- [30] J.E.Martin, J.Odinek and T.C.Halsey, Phys.Rev.Lett. **69**, 1524 (1992).
- [31] J.M.Laskar, J.Philip and B.Raj, Phys.Rev.E **82**, 021402 (2010).
- [32] J.J.M.Janssen, J.J.M.Baltussen, A. Gelder and J.A.A.J.Perenboom, J.Phys.D: Appl. Phys. **23**, 1447 (1990).
- [33] M.Hagenbuechle and J.Liu, Appl. Opt. **36**, 7664 (1997).
- [34] C.P.Reynolds, D.R.Robinson, D.G.A.L.Aarts, M.Wilson, W.W.Sampson and R.P.A.Dullens, Euro. Phys. Lett. **116**, 0295 (2016).
- [35] D. Gennes and Pincus, Phys. Kondens. Mat. **11**, 189 (1970).
- [36] P.C.Jordan, Mol. Phys. **38**, 769 (1979).
- [37] J.P. Hansen and I. McDonald, *Theory of Simple Liquids* (, , 1986).
- [38] N. March and M.P.Tosi, *Coulomb Liquids* (, , 1984).
- [39] M. Leeuwen and B.Smit, Phys. Rev. Lett. **71**, 3991 (1993).
- [40] T.Tlusty and S.A.Safran, Science **290**, 1328 (2000).
- [41] D.Wei and G.N.Patey, Phys. Rev. Lett **68**, 2043 (1992).
- [42] D.Levesque and J.J.Weis, Phys. Rev. E **49**, 5131 (1994).

- [43] J.J.Weis and D.Levesque, Phys. Rev. E **48**, 3728 (1993).
- [44] J.J.Weis and D.Levesque, Phys. Rev. Lett. **71**, 2729 (1991).
- [45] D.Wei and G.N.Patey, Phys. Rev. A **46**, 7783 (1992).
- [46] J.J.Weis, D.Levesque and G.J.Zarragoicoechea, Phys. Rev. Lett. **69**, 913 (1992).
- [47] J.-J.Weis, Mol. Phys. **103**, 7 (2005).
- [48] H.Schmidle and S.H.L.Klapp, J. Chem. Phys. **134**, 114903 (2011).
- [49] E.A.Elifimova, A.O.Ivanov and P.J.Camp, J. Chem. Phys. **136**, 194502 (2012).
- [50] E.A.Elifimova, A.O.Ivanov and P.J.Camp, Phys. Rev. E **86**, 021126 (2012).
- [51] J.J.Weis and D.Levesque, J. Chem. Phys. **125**, 034504 (2006).
- [52] G.Ganzenmueller, G.N.Patey and P.J.Camp, Mol. Phys. **107**, 403 (2009).
- [53] X.S.Chen, M.Kasch and F.Forstmann, Phys. Rev. Lett. **67**, 2674 (1991).
- [54] X.S.Chen and F.Forstmann, Mol. Phys. **76**, 1203 (1992).
- [55] A.F.Pshenichnikov and V.V.Mekhonoshin, Eur. Phys. J. E **6**, 399 (2001).
- [56] N.G.Almarza, E.Lomba, C.Martin and A.Gallardo, J. Chem. Phys. **129**, 234504 (2008).
- [57] A.Goyal, C.K.Hall and O.D.Velev, J. Chem. Phys. **133**, 064711 (2010).
- [58] P.H.Lee and B.M.Ladanyi, J. Chem. Phys. **91**, 7063 (1989).
- [59] S. Leeuw, B.Smit and C.P.Williams, J. Chem. Phys. **93**, 2704 (1990).
- [60] G.C.A.M.Mooij, S. Leeuw, C.P.Williams and B.Smit, Mol. Phys. **71**, 909 (1990).
- [61] G.C.A.M.Mooij, S. Leeuw, B.Smit and C.P.Williams, J. Chem. Phys. **97**, 5113 (1992).
- [62] A.Mueller, J.Winkelmann and J.Fischer, Fluid Phase Equil. **99**, 35 (1994).
- [63] C.Kriebel, A.Mueller, J.Winkelmann and J.Fischer, Fluid Phase Equil. **119**, 67 (1996).
- [64] A. Mueller, J.Winkelmann, T.Boublik and J.Fischer, Mol. Phys. **78**, 121 (1993).
- [65] G.M.Range and S.H.L.Klapp, Phys. Rev. E **69**, 041201 (2004).
- [66] M.J.Blair and G.N.Patey, Phys. Rev. E **57**, 5682 (1998).
- [67] E.L.Pollock, B.J.Alder and G.N.Patey, Physica **108A**, 14 (1981).
- [68] J.M.Caillol, D.Levesque, J.J.Weis, P.G.Kusalik and G.N.Patey, Mol. Phys. **55**, 65 (1985).
- [69] S.Dobra, I.Szalai and S.Varga, J. Chem. Phys. **125**, 074907 (2006).
- [70] C.Brunet, J.G.Malherbe and S.Amokrane, Phys. Rev. E **82**, 021504 (2010).
- [71] K. Barros and E. Luijten, Phys. Rev. Lett. **113**, 017801 (2014).
- [72] K. Barros, D. Sinkovits and E. Luijten, J. Chem. Phys. **140**, 064903 (2014).
- [73] J. Qin, J. Li, V. Lee, H. Jaeger, J. de Pablo and K.F.Freed, J. Colloid and Int. Sci. **469**, 237 (2016).
- [74] A.Bradbury, S.Menear and R.W.Chantrell, J. Mag. Mag. Mat. **54-57**, 745 (1986).
- [75] B. Cabral, J. Chem. Phys. **112**, 4351 (2000).
- [76] T.Kruse, A.Spanoudaki and R.Pelster, Phys. Rev. B **68**, 054208 (2003).
- [77] A.O.Ivanov and S.S.Kantorovich, Coll. Jour. **65**, 166 (2003).
- [78] A.O.Ivanov and S.S.Kantorovich, Phys. Rev. E **70**, 021401 (2004).
- [79] Z.Wang and C.Holm, Phys. Rev. E **68**, 041401 (2003).
- [80] A.O.Ivanov, J. Mag. Mat. **154**, 66 (1996).
- [81] R. Car and M.Parrinello, Phys. Rev. Lett. **55** (22), 2471 – 2474 (1985).
- [82] D.K. Remler and P.A. Madden, Mol. Phys. **70** (6), 921–966 (1990).
- [83] P.A.Madden and M. Wilson, Chem. Soc. Rev. **25**, 339 (1996).
- [84] S. Nosé, J. Chem. Phys. **81**, 511 (1984).
- [85] W.G. Hoover, Phys. Rev. A **31**, 1695 (1985).
- [86] S.L. Roux and P. Jund., Comp. Mat. Sci. **49**, 70 (2010).
- [87] C.P.Reynolds, *D.Phil Thesis* (, , 2016).
- [88] E. Rapaport, Journal of Chemical Physics **46** (8), 2891–2895 (1967).
- [89] E. Rapaport, Journal of Chemical Physics **48** (4), 1433–1437 (1968).
- [90] E.A. Guggenheim, *Modern thermodynamics by the methods of Willard Gibbs* (Methuen & co. ltd., London,, 1933).

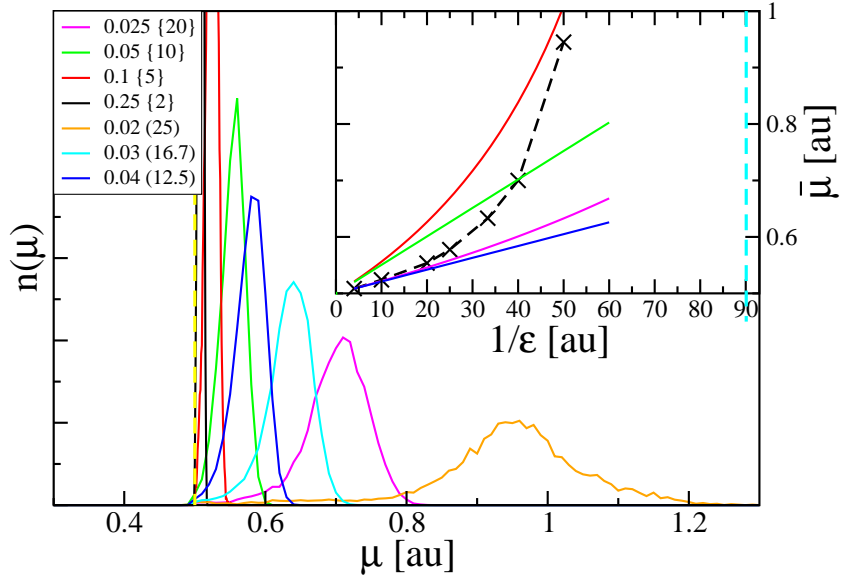


Figure 1. (Main panel) Distribution of dipole moments calculated by averaging over 50 quenched configurations at seven different combinations of external fields and atom polarizabilities (shown as $\epsilon(\alpha)$ in the figure legend) in atomic units. In all cases the product $\mu^{ex} = \alpha\epsilon^{ex}$ is held fixed at 0.5au. The inset shows the mean dipole (\times) as a function of the applied field along with the total dipoles predicted for a pair of atoms and for an infinite chain for a first-order corrected DID term and the full self-consistent term. **Key:** red - chain, self-consistent, green - chain, first-order, magenta - two atoms, self consistent, blue - two atoms, first order. The vertical line in the inset highlights the theoretical field below which a polarization catastrophe occurs.

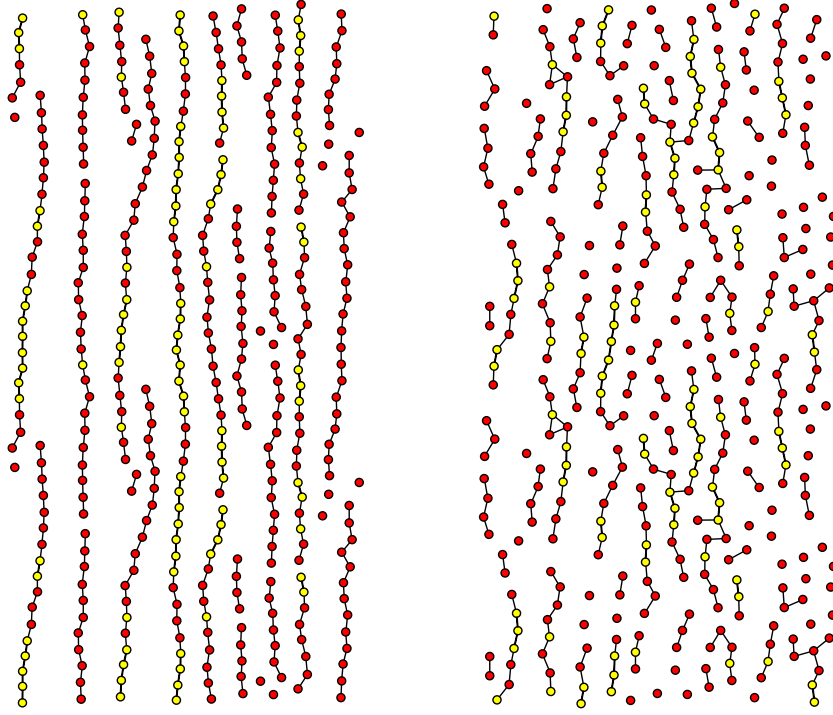


Figure 2. Molecular graphics “snapshots” for the monodisperse system at low field (left panel, $\epsilon = 0.025\text{au}$, $\alpha = 20\text{au}$) and high field (right panel $\epsilon = 0.25\text{au}$, $\alpha = 2\text{au}$) respectively for $\mu^{ex} = 0.5\text{au}$. The direction of the applied field is shown by the arrow. In both panels the light circles highlight the atoms with dipoles of magnitude in the upper 25% of the dipole distribution (figure 1) whilst the dark circles highlight the position of the remaining atoms which have smaller dipole moments.

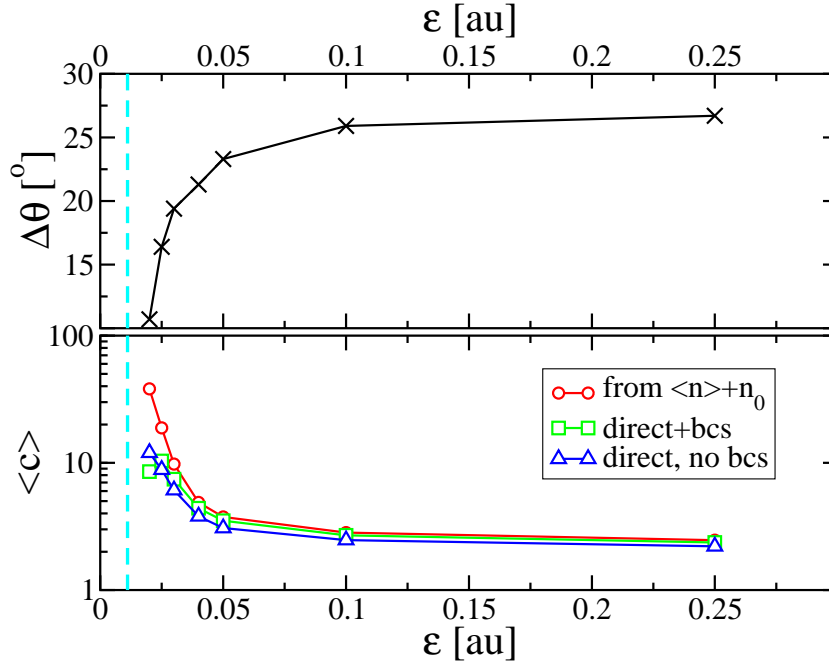


Figure 3. (Upper panel). Half width at half maximum peak widths for the bond angle distributions calculated for all atoms as a function of the external field, determined at fixed $\mu = \alpha\epsilon^{ex}$. As the external field is reduced (α increased) the peaks become narrower indicative of greater chain ordering with respect to the applied external field vector. (Lower panel). Mean chain lengths calculated as a function of the external field at fixed $\mu = \alpha\epsilon^{ex}$. As the external field is reduced (α increased) the mean chain lengths increase significantly. The chain lengths are calculated in three different ways as described in the text. Key: \circ - calculated from the mean coordination number (equation 16), \square - calculated by direct counting of the chain lengths including the periodic boundary conditions, \triangle - calculated by direct counting without applying the boundary conditions.

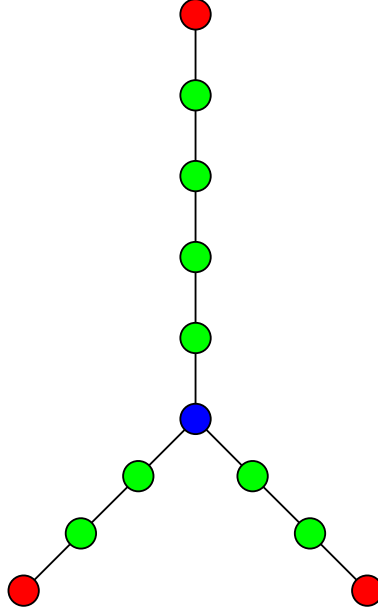


Figure 4. A small cluster to highlight the “shortest chain approximation” definition applied to calculate the chain length distributions in the present work. The singly- and three-coordinate atoms are defined as chain termini meaning that this cluster is reported as comprised of one 6 atom chain and two 4 atom chains.

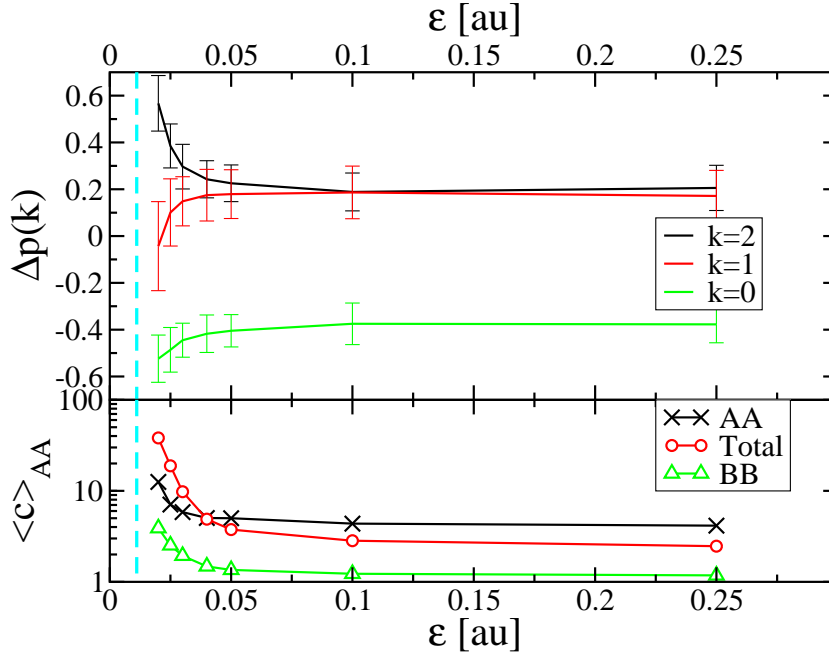


Figure 5. (Upper panel). Coordination difference functions (normalised by limits assuming all in AAA chains). $\Delta p(2)$ increases as the external field falls corresponding to greater chain formation associated with dipole-induced dipole effects. (Lower panel). Mean chain lengths (determined from the mean coordination numbers - equation 16) for all atoms (\circ) and those composed of atoms A (\times) and B (\triangle) only.

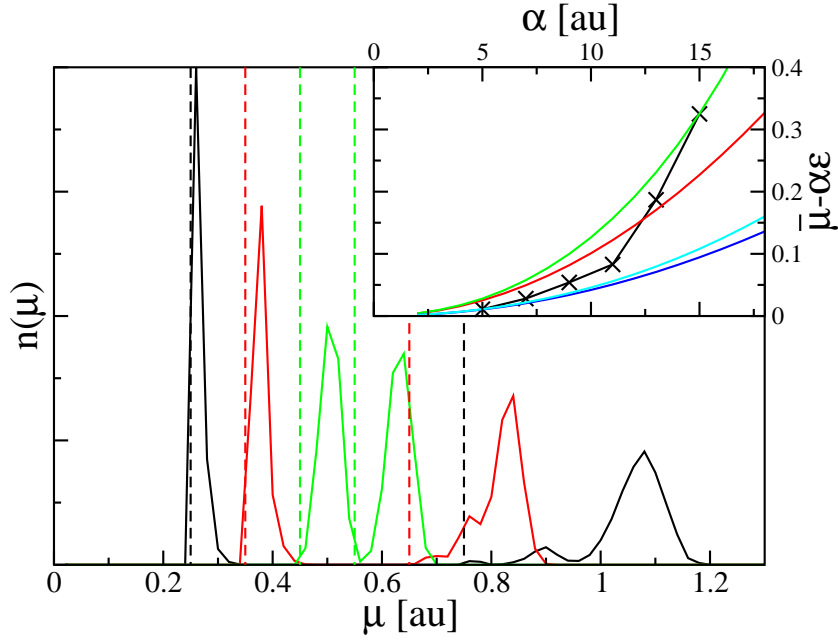


Figure 6. Distribution of dipole moments averaged over 50 quenched configurations for a fixed applied field of $\epsilon^{ex} = 0.05\text{au}$. Three sets of polarizabilities $\{\alpha_1, \alpha_2\}$ as shown; {15, 5}, {13, 7} and {11, 9} (black, red and green lines respectively). The dashed vertical lines indicate the values of the dipoles in the absence of any dipole-induced dipole (DID) effects. The inset shows the "excess" mean dipole (effectively the DID) as a function of polarizability (black crosses) compared to ideal values predicted for an isolated atom pair and the infinite chain at the first order and self-consistent limits. **Key:** green - chain, self consistent, red - chain, first-order, cyan - two atoms, self consistent, blue - two atoms, first order.

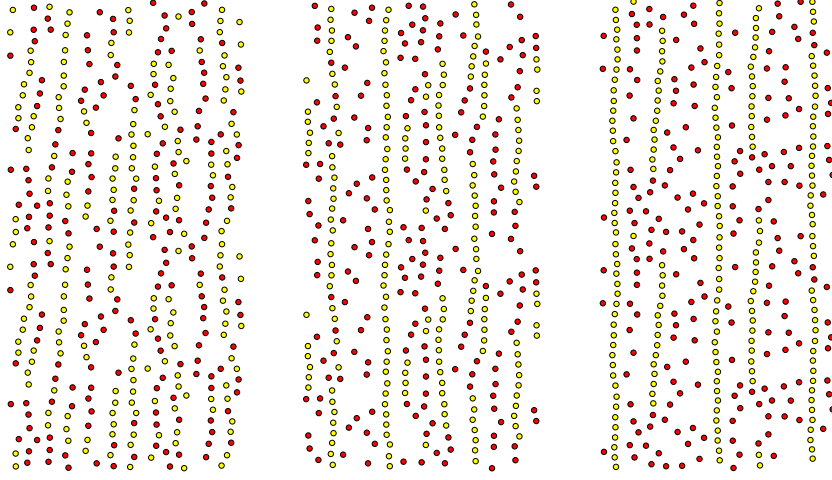


Figure 7. Molecular graphics “snapshots” for three configurations at an external field of $\epsilon^{ex} = 0.05\text{au}$. The direction of the applied field is shown by the arrow. The left panel is for a configuration with polarizabilities $\{\alpha_1, \alpha_2\} = \{11, 9\}\text{au}$, the central panel is for $\{\alpha_1, \alpha_2\} = \{13, 7\}\text{au}$ whilst the right panel is for $\{\alpha_1, \alpha_2\} = \{15, 5\}\text{au}$. In all panels the more polarizable species are shown as light circles and the less polarizable species as dark circles.

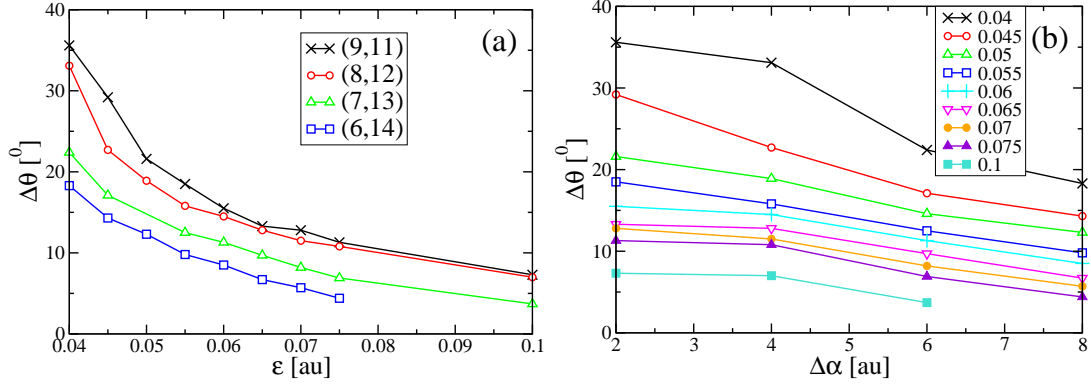


Figure 8. (a) HWHM for the bond-angle distributions (BADs) as a function of external field for four sets of $\{\alpha_1, \alpha_2\}$ (indicated in au) with $\bar{\alpha} = 10\text{au}$. (b) HWHM for the same BADs plotted as a function of the polarizability contrast, $\Delta\alpha$, at fixed external fields as indicated (in au).

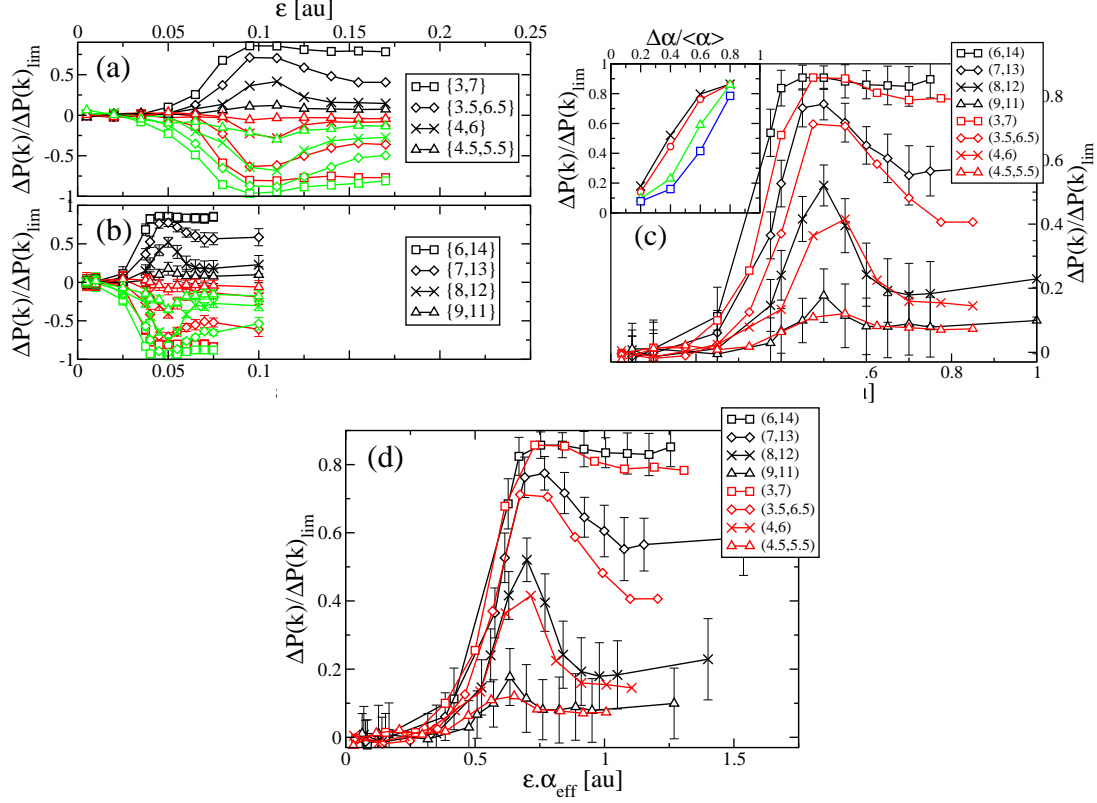


Figure 9. (a) and (b) Coordination number difference functions, $\Delta p(k)$ [$k = 0, 1, 2$] for A atoms at the centre as a function of external field for (lower panel) four sets of $\{\alpha_1, \alpha_2\}$ (indicated in au) with $\bar{\alpha} = 10$ au and for (upper panel) three sets of $\{\alpha_1, \alpha_2\}$ (indicated in au) with $\bar{\alpha} = 5$ au. **Key: black, green and red lines correspond to $k = 2, 1$ and 0 respectively.** (c) [Main panel] Coordination number difference functions, $\Delta p(2)$ for A atoms at the centre as a function of external field for seven sets of $\{\alpha_1, \alpha_2\}$ (indicated in au). The applied field is scaled by the mean polarizability, $\bar{\alpha}$. The inset shows the peak heights and high field limits as a function of $\Delta\alpha/\bar{\alpha}$. Key: crosses - peak maxima (10au), circles - peak maxima (5au), triangles - high field limit (10au), squares (5au). (d) Coordination number difference functions scaled in terms of an effective polarizability (which incorporates the first order DID terms) as discussed in the text.

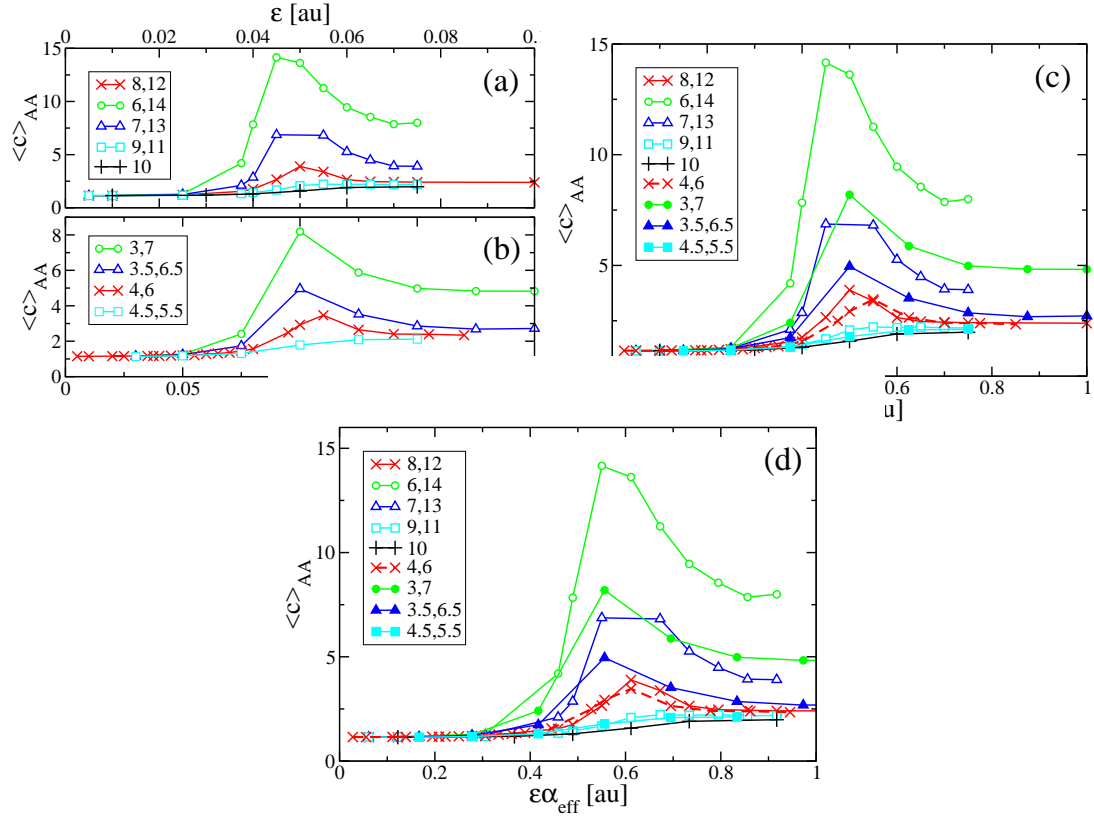


Figure 10. Mean chain lengths for chains containing A-atoms only. In (a) and (b) these are shown as a function of the magnitude of the external field for $\bar{\alpha} = 10\text{au}$ and $\bar{\alpha} = 5\text{au}$ respectively with the specific $\{\alpha_1, \alpha_2\}$ pairs as indicated. In (c) and (d) the two data sets are plotted on the same figures as a function of the field scaled by the mean polarizability and effective polarizability respectively.

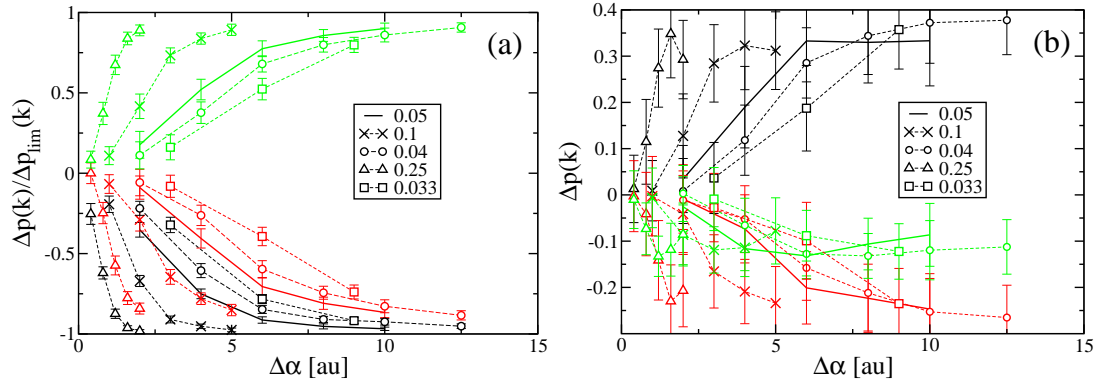


Figure 11. Coordination number difference functions, $\Delta p(k)$ [$k = 0, 1, 2$] for (a) A atoms at the centre, (b) B atoms at the centre for the external fields indicated (in au). In both (a) and (b) these are plotted as a function of the polarizability contrast, $\Delta\alpha$. Key: black, red and green lines correspond to $k = 0, 1$ and 2 respectively.

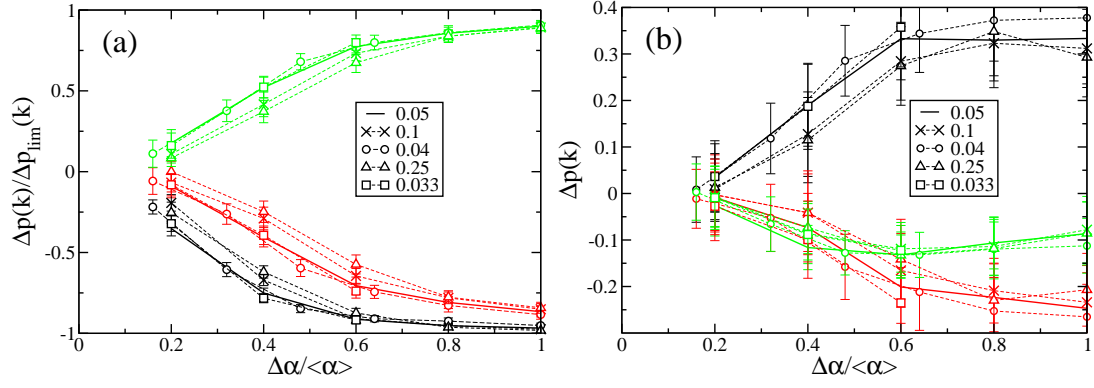


Figure 12. Coordination number difference functions, $\Delta p(k)$ [$k = 0, 1, 2$] for (a) A atoms at the centre, (b) B atoms at the centre for the external fields indicated. The abscissa is scaled by $\Delta\alpha/\bar{\alpha}$ as discussed in the text. Key: black, red and green lines correspond to $k = 0, 1$ and 2 respectively.

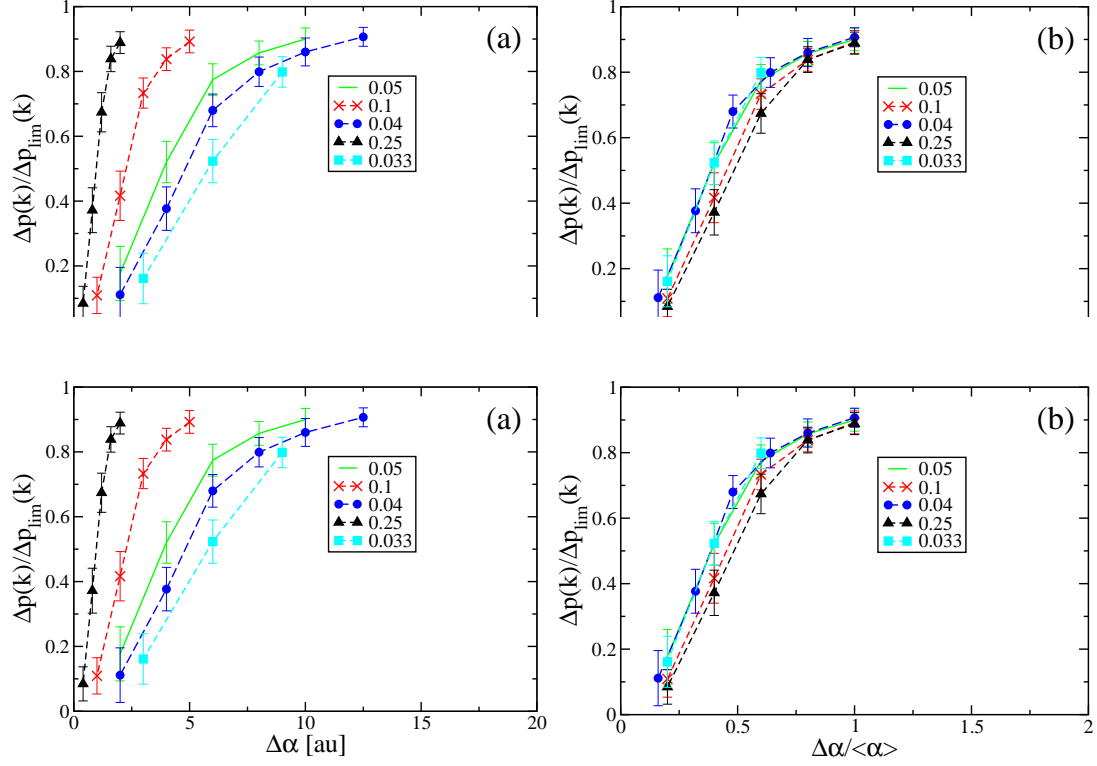


Figure 13. Coordination number difference functions, $\Delta p(2)$ for A atoms at the centre determined for the external fields as indicated. Panels (a) and (c) show the data as a function of the polarizability and effective polarizability contrasts respectively. Panels (b) and (d) show the data scaled by $\Delta\alpha/\bar{\alpha}$ and $\Delta\alpha_{\text{eff}}/\bar{\alpha}_{\text{eff}}$ respectively.

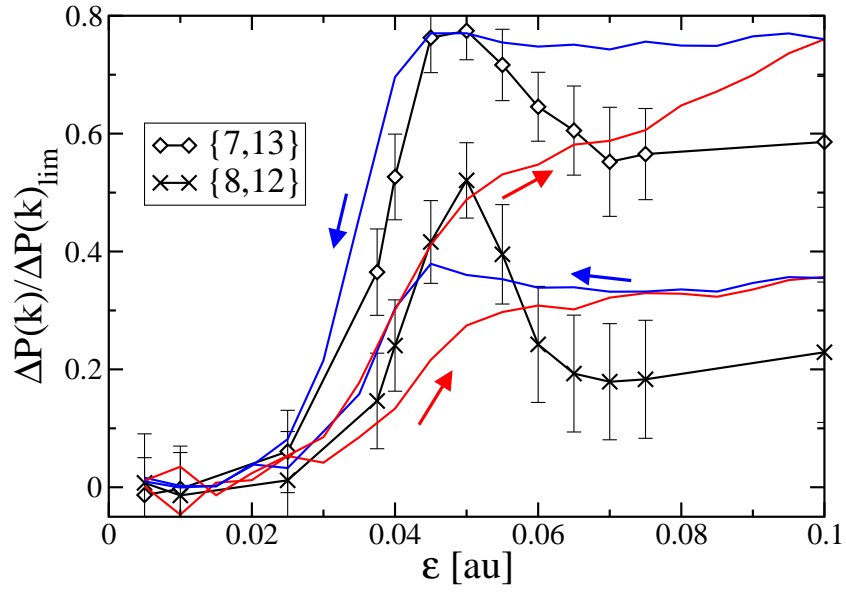


Figure 14. Coordination number difference functions, $\Delta p(2)$ for two pairs of $\{\alpha_1, \alpha_2\}$ as indicated. The black lines show the results from quenching from isotropic configurations at fixed external field, whilst the red and blue lines show the result of ramping the external field upwards and downwards (as emphasized by the arrows).